

# THE CRYSTAL BALL HYPOTHESIS IN DIFFUSION MODELS: ANTICIPATING OBJECT POSITIONS FROM INITIAL NOISE

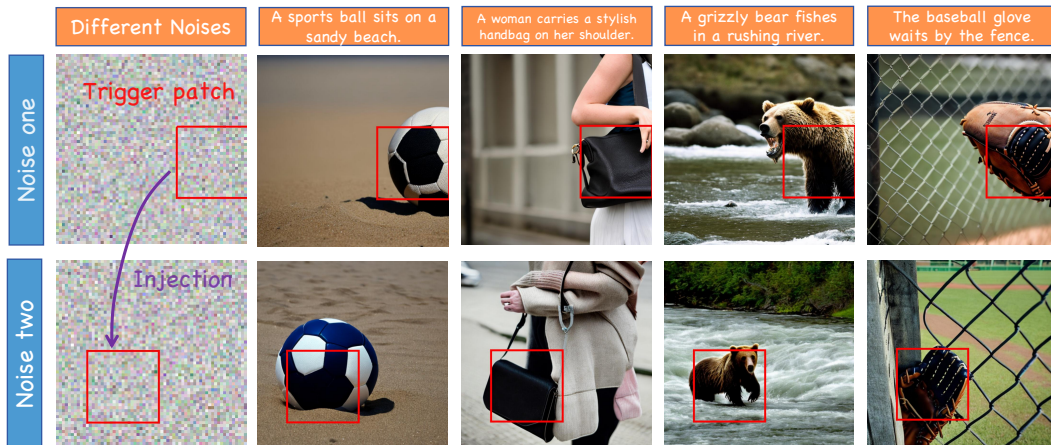
006 **Anonymous authors**

007 Paper under double-blind review

## ABSTRACT

013 Diffusion models have achieved remarkable success in text-to-image generation  
 014 tasks, yet the influence of initial noise remains largely unexplored. In this study,  
 015 we identify specific regions within the initial noise image, termed trigger patches,  
 016 that play a key role in inducing object generation in the resulting images. Notably,  
 017 these patches are **universal** and can be generalized across various positions, seeds,  
 018 and prompts. To be specific, extracting these patches from one noise and injecting  
 019 them into another noise leads to object generation in targeted areas. To identify  
 020 the trigger patches even before the image has been generated, just like consulting  
 021 the crystal ball to foresee fate, we first create a dataset consisting of Gaussian  
 022 noises labeled with bounding boxes corresponding to the objects appearing in  
 023 the generated images and **train a detector that identifies these patches from**  
 024 **the initial noise**. To explain the formation of these patches, we reveal that they  
 025 are **outliers** in Gaussian noise, and follow distinct distributions through two-  
 026 sample tests. These outliers can take effect when injected into different noises and  
 027 generalize well across different settings. Finally, we find the misalignment between  
 028 prompts and the trigger patch patterns can result in unsuccessful image generations.  
 029 To overcome it, we propose a reject-sampling strategy to obtain optimal noise,  
 030 aiming to improve prompt adherence and positional diversity in image generation.

## 1 INTRODUCTION



048 Figure 1: The first row displays images generated from the same seed, where the “trigger patch” can  
 049 be identified within the red box, indicating its tendency to induce object generation. When this trigger  
 050 patch is injected into another noise pattern, objects will appear in the corresponding position within  
 051 the images generated from the mixed noise. Please refer to Fig 15 for more examples.

052 In recent years, diffusion models have revolutionized the field of text-to-image generation (Saharia  
 053 et al., 2022; Rombach et al., 2022; Dhariwal & Nichol, 2021; Nichol et al., 2021; Ho & Salimans,  
 2022). However, these models often fail to accurately adhere to the prompts, frequently generating

054 objects with specific positions or attributes regardless of the input text (Chefer et al., 2023; Hertz  
 055 et al., 2022; Wang et al., 2022). Despite various methods aimed at enhancing control over the  
 056 generation process have been introduced, including modifying the denoising process (Balaji et al.,  
 057 2022), manipulating cross-attention layers (Hertz et al., 2022; Feng et al., 2022), and retraining models  
 058 using layout-image pairs (Zheng et al., 2023; Zhang et al., 2023; Voynov et al., 2023). Nonetheless, a  
 059 key question remains unanswered: *Why is the generation process so difficult to control?*

060 In this paper, we show that Gaussian noise in the diffusion process plays a crucial role in image  
 061 generation. Specifically, we discover the existence of **trigger patches** – distinct patches in the noise  
 062 space that trigger the generation of objects in the diffusion model. By moving the trigger patch to a  
 063 different position, the corresponding object will likely move to that location. Furthermore, this effect  
 064 also exists across various prompts—the same trigger patch can initiate the generation of different  
 065 objects, depending on the given prompt. These phenomena are illustrated in Figure 1: when replacing  
 066 the target patch within **another initial noise** with the trigger patch, the injection position would  
 067 generate an object. Identifying the location of trigger patches can provide insights into where objects  
 068 will be generated **without running the diffusion process**. Moreover, moving/removing trigger  
 069 patches can achieve certain image editing effects.

070 *How can we find trigger patches?* Our ultimate goal is to obtain a **Crystal Ball** that can anticipate the  
 071 position of the objects in the generated images even before the diffusion process. We first propose a  
 072 posterior approach based on the following intuition: given a specific initial noise, if all the objects  
 073 are confined to a specific location regardless of the prompts, there must be a trigger patch in the  
 074 corresponding position. Hence, we try to identify trigger patches by calculating the variance of  
 075 coordinates of detected objects in the generated images. *But can we detect trigger patches without*  
 076 *actually running a diffusion process?* To achieve that, we propose a “trigger patch detector”, which  
 077 functions similarly to an object detector but operates in the noise space. Our trigger patch detector,  
 078 functioning like a crystal ball, achieves an mAP50 of 0.333 on the validation set<sup>1</sup>, revealing that  
 079 trigger patches are ignorant of specific prompts and noises.

080 *So what makes trigger patches special?* We hypothesize that the trigger patches are **outliers** within  
 081 the Gaussian noise. We perform a two-sample test comparing the trigger patches to randomly selected  
 082 noise patches and confirm that they follow distinct distributions. In particular, more effective trigger  
 083 patches show greater divergence from the standard Gaussian distribution. To further support our  
 084 claim, we design some handcrafted trigger patches shifted from the original distribution. We validate  
 085 that they effectively trigger object formation at corresponding positions in the generated images.

086 Finally, we demonstrate two applications of trigger patches. For scenarios when location information  
 087 is specified in the prompt, we show that designing noises with trigger patches at the target location can  
 088 significantly boost the generation success rate from 57.08% to 83.64%. Conversely, for applications  
 089 when location diversity of generated objects is preferred, we demonstrate that using our proposed  
 090 detector to “purify” the noise can significantly increase generation diversity.

## 091 2 TRIGGER PATCHES DETERMINE GENERATED LOCATIONS

### 092 2.1 PRELIMINARIES

093 **Denoising Diffusion Probabilistic Models (DDPM)** DDPM (Ho et al., 2020) is a kind of generative  
 094 model, which achieves great performance on high-quality image synthesis. The inference process  
 095 initiates with the standard Gaussian noise  $x_T$  and iteratively applies the model to progressively  
 096 denoise it back towards the natural image  $x_0$  that subjects to the real data distribution.

097 **Classifier-free guidance for conditional generation** Text-to-image diffusion models incorporate  
 098 classifier-free context information into the reverse diffusion process via cross-attention layers. Specif-  
 099 ically, at each sampling step, the denoising error is calculated by adjusting the conditional error with  
 100 an unconditional error, factored by a guidance strength.

### 102 2.2 DEFINITION OF TRIGGER PATCH

104 Where will a diffusion model position an object in the generated images? In this section, we  
 105 show that *the initial noise takes an important role in generated objects’ location*. Specifically,  
 106 we identify regions within the initial noise, termed “**trigger patches**”, that largely determine the  
 107

<sup>1</sup>Faster R-CNN Ren et al. (2015) achieves a mAP<sub>50</sub> of 0.596 on COCO validation set Lin et al. (2014).



Figure 3: Illustration: Each row shows five images generated from one seed. The patch in the bottom row has the strongest effectiveness in inducing the generation of the object, while the objects in the top row are dispersed. So there must exist a strong trigger patch in the orange bounding box in the bottom row noise.

object location. Formally, a trigger patch is a patch in the noise space with the following properties: (1) Triggering Effect: When it presents in the initial noise  $Z_0$ , the trigger patch consistently induces object generation at its corresponding location; (2) Universality Across Prompts: The same trigger patch can trigger the generation of various objects, depending on the given prompt.

Specifically, for a fixed initial noise, we generate 25 images with various prompts, and then detect the object in each generated image. Please refer to Appendix B for more details. By summing the object masks and normalizing the results, we generate a heatmap where each pixel represents the probability of an object appearing at that location. Fig 2 demonstrates the heatmaps for two different noises. For the image on the left, all generated objects are concentrated in roughly the same location with high probability, indicating the presence of a trigger patch that consistently drives object generation at that location. Conversely, the right heatmap has no such an obvious pattern, suggesting no trigger patch in that particular noise.

To formulate a quantitative expression, we can first use a pre-trained detector to obtain the coordinates of the bounding boxes  $\{(x_1, y_1, x_2, y_2)\}$ , where  $(x_1, y_1)$  represents the coordinates of the upper-left corner, and  $(x_2, y_2)$  represents the coordinates of the lower-right corner of the bounding box. Then, we can define a posterior metric about the effectiveness of the regions in inducing objects, termed “trigger entropy”. For each initial noise, the more concentrated the boxes are, the smaller trigger entropy it has. To avoid the bias of the object size, we compute the center point of each object bounding box  $x_c = \frac{x_1+x_2}{2}$  and  $y_c = \frac{y_1+y_2}{2}$ . Then the entropy of the patch can be defined based on the variance of the box centers:

$$\mathcal{H}(X) = \frac{1}{2} \left( \frac{1}{n} \sum_{i=1}^n (x_{c_i} - \bar{x}_c)^2 + \frac{1}{n} \sum_{i=1}^n (y_{c_i} - \bar{y}_c)^2 \right) \quad (1)$$

where  $\bar{x}_c = \frac{1}{n} \sum_{i=1}^n x_{c_i}$ ,  $\bar{y}_c = \frac{1}{n} \sum_{i=1}^n y_{c_i}$ , and  $i$  is the box index. So, the more entropy a region has, the less effective it is in determining the objects’ locations, as shown in Fig 3.

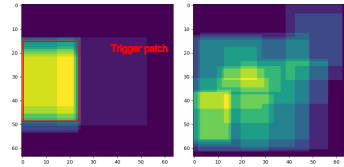


Figure 2: Heatmaps of generated objects on two different noises. The left one has a trigger patch while the right one does not. Please refer to Fig 8 for more visualized results.

### 3 THE CRYSTAL BALL: DETECTING TRIGGER PATCHES FROM NOISE

### 3.1 TRAINING A CRYSTAL-BALL DETECTOR

The above method requires generating images to identify trigger patches. *Can we detect the trigger patches without running the diffusion process, just like looking into the Crystal Ball to anticipate it?* To answer this question, we try to train a trigger patch detector, which functions similarly to an object detector but operates in the noise space.

**Generating Noise-Annotations Dataset** To train a detector, we generate a dataset consisting of initial noises paired with the bounding boxes of objects in the corresponding images. Initially, we select five classes from the COCO dataset: “stop sign, bear, sports ball, handbag, and apple”. We then prompt ChatGPT to generate five unique sentences for each class, ensuring each sentence features only one object to prevent duplicates. Please refer to Appendix B for the prompt used for ChatGPT and the 25 prompts used to generate images. We sample 20,000 Gaussian noises and use diffusion models to generate images based on these noises and prompts. A pre-trained object detector from MMDetection (Chen et al., 2019) is then applied to identify the object bounding boxes, which are resized from the image space to the latent space. Only the bounding box with the highest score and correct object label is retained for each image. Please refer to Appendix B for more details about the image generation settings and the detection settings.

**Detection Dataset** We divide 20,000 random noises into a training set (17,500), a validation set (1,000), and a test set (1,500). Subsequently, we modify the trigger patch annotations to create four distinct datasets, the details of which are presented in Table 1. The *Augmented* dataset uses bounding boxes of all the 25 prompts, while the *Restricted* only uses those of the class “sports ball”. In the *Class-Specific* dataset, the model is required to output the class labels of the trigger patch. Additionally, we craft a *Shuffled* dataset with shuffled annotations to serve as a baseline to mitigate the effects of other bias. For example, if we use an biased training dataset with all the objects appearing in one place, a detector simply outputs center boxes constantly can achieve good results. We call it model and prompt bias. So we propose to shuffled the annotations of the data, as Fig 9 shows. If all bounding boxes are centralized, the training outcomes on the Shuffled dataset should align with those from the Restricted dataset.

Table 1: Dataset Description

Dataset	Classes	Annotations per noise	Output classes	Shuffled annotations
Restricted	Sports ball	$5 = 1 \times 5$	×	×
Augmented	All	$25 = 5 \times 5$	×	×
Class-Specific	All	$25 = 5 \times 5$	✓	×
Shuffled	Sports ball	$5 = 1 \times 5$	×	✓

**Results** We utilize the MMDetection repository to train our trigger patch detector. Please refer to Appendix D for more details about training recipe. The results can be seen in Table 2. **Our detector on Restricted achieves the mAP<sub>50</sub> of 0.325, surpassing the Shuffled baseline by 0.124.** Such evidence eliminates the influence of the model bias and prompt bias, verifying that the model has learned to locate the trigger patches from initial noises. Please refer to the Appendix D for more comparison with detectors on standard COCO dataset. Notably, the results on the Augmented dataset show that the trigger patches can generalize across different text prompts and provide a foundation for the applications of our detector in various scenarios. Meanwhile, the detector on Class-Specific dataset shows degenerated performance, indicating that the trigger patches are ignorant of the classes and universal across prompts. In other words, these patches can only determine where objects are generated, not what to generate.

Table 2: Training a detector to anticipate object positions from initial noise.

Dataset	Restricted	Augmented	Class-Specific	Randomized
mAP <sub>50</sub>	0.325	0.333	0.091	0.201

216

### 3.2 THE UBIQUITOUS AND DIVERSITY OF TRIGGER PATCH

217

In this subsection, we perform a series of studies to address the following questions: **1) Dataset statistics:** How frequently do trigger patches appear in the initial noise? **2) Generalization:** Can trigger patches generalize effectively across various noises, sampling configurations (.schedulers, sampling steps, and aspect ratios) and different model types (LoRA models, fine-tuned models, and others)? **3) Trigger-prompt interaction:** How does the interaction between the trigger patch and prompt affect performance, especially when the prompt includes positional information that contradicts or aligns with the trigger patch location? **4) Multiple trigger patches:** What happens when a noise contains multiple trigger patches? **5) Trigger patch preference:** Do trigger patches show a preference for certain object categories?

226

**Dataset Statistics** We compute the trigger entropy defined in equation 1 for all the 20,000 noises and plot the histograms in Fig 4. We first study a trivial case, where we compute the trigger entropy based on the boxes of one class, “sports ball”, and five prompts about this class. Then, for a more general one, we compute the trigger entropy based on all 5 classes and 25 prompts to see if the metric can generalize well across various prompts and classes. As shown in Fig 4, nearly 10% of the noises in the first group have an entropy near 0. In other words, for nearly 2,000 noises, sports balls always show up in almost the same place across the five images generated from an initial noise, indicating that strong trigger patches are very common in initial noises.

235

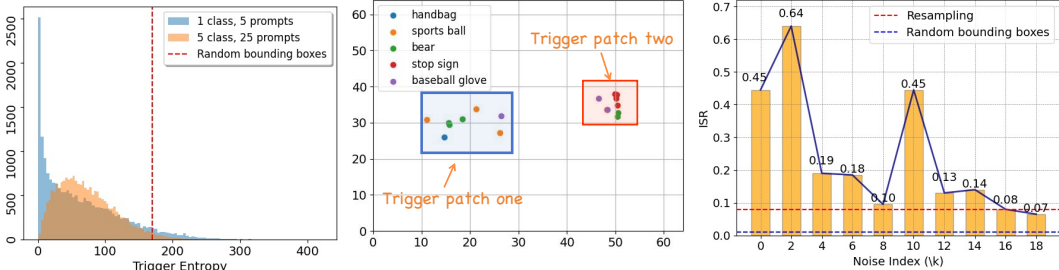


Figure 4: Trigger Entropy Distribution on the created dataset. For one noise, we plot the scatter plot of trigger entropy and do injection experiments on every 2000 noise.

248

**Generalization** We design an **Trigger Injection** experiment to test if these patches can still take effect when injected into another noise. In particular, we replace an arbitrary patch in a noise map with the trigger patch and then use the blended noise for generation. A successful injection is characterized by the detected bounding box occupying more than 75 percent of the trigger patch region. Then we define the injection success rate (ISR) as the ratio of successful injection cases to the total number of cases. We sort the patches in our dataset by trigger entropy and select one every two thousand for this test. We do the injection experiment with 200 new random noises. There are two baselines as follows. 1) Resampling: Resample Gaussian noise for the target region maintaining the same mean and variance. 2) Random: Select a random patch within a source noise, which might overlap with the trigger patch in the source noise. Figure 6 illustrates that the Injection Success Rates (ISRs) of most trigger patches exceed those of the Resampling (0.08) and Random (0.01) baselines, confirming the efficacy of the trigger patches. Additionally, a lower trigger entropy correlates with a higher ISR, suggesting that the trigger patches with low entropy are particularly effective in determining object locations. Moreover, to verify the trigger patches are “universal” and can **generalize well across different sampling timesteps, samplers, aspect ratios, fine-tuned models and LoRA models**, we conduct a series of additional Trigger Injection experiments with different configurations and models. Please refer to the Appendix C for more ablation study on generalization.

265

**Trigger-Prompt Interaction** The ability of trigger patches to introduce positional information raises an important question: What happens when prompts also include positional cues, and how do the prompt and noise interact when their object positions are **either aligned or in conflict**? To explore this, we first design prompts with the format of “a coco class name on the right side”. Then we select three noises: 1) Aligned: with a strong trigger patch on the right, 2) Contradicted: with a strong trigger patch on the left, and 3) Dispersed: with trigger patches dispersed throughout the image.

After viewing the generated images, we divided them into four groups: 1) Aligned: The position of the object is aligned with the prompt guidance (On the right side). 2) Contradicted: The position of the object contradicts with the prompt guidance (On the left side). 3) Duplicated: the generated image has two objects on both sides. Please refer to Fig 14 for more details. 4) Hard to judge (Occupying the entire picture, failed generation, or in the middle of the image). [Please to Appendix H for a failed analysis.](#) Table 3 demonstrates that the trigger patches significantly influence the final positions

Table 3: Diversity Results

Noise	Aligned (%)	Contradicted (%)	Duplicated (%)	Hard to judge (%)
Aligned	63.5	6.3	6.3	23.9
Contradicted	35.0	32.5	8.8	23.7
Dispersed	25.0	10.0	11.3	53.7

of objects. When the prompt and trigger patches are contradictory, 32.5% of objects adhere to the trigger patches, while only 35.0% follow the prompt’s guidance, highlighting the prevalence of failed generations due to **conflicts between the prompt and initial noise about where to position objects**. Notably, when the prompt and trigger patches are aligned, 63.5% of objects are accurately positioned. These results indicate the potential to manipulate trigger patches for controlled image generation, as demonstrated in Section 5.2.

**Multiple trigger patches within a noise** It contains two questions. **1) Can multiple trigger patches appear in one noise?** To answer the question, we plot the center points of the detected bounding boxes of one specific noise in Fig 5. As shown, two distinct clusters are present, indicating the existence of multiple trigger patches within a single noise. **2) Can noises with multiple trigger patches benefit multiple object generation performance?** We conduct a series of experiments using the prompts like “a lion and a yellow clock”. **We find the presence of multiple trigger patches enhances multiple object generation performance.** Please refer to the Appendix G for more details.

**Trigger Patch preference** The trigger patches themselves have no significant preference for certain kinds of objects and does not depend on the specific prompt — both trigger patches in Fig 5 can generate baseball gloves (purple points) and bears (green points). However, we do observe some indications of positional preference, as certain objects are more likely to generate within the trigger patches located at specific positions, revealing a position bias of these object classes. As shown in Fig 5, handbags only appeared in the bottom left region, while stop signs appeared only in the upper right region. **We attribute this preference to the position of the trigger patch within the initial noise, rather than the properties of the patch itself.** In the real-world distribution, most stop signs are located in the upper part of the image, while most handbags are in the lower part. This likely causes them to favor trigger patches in certain positions. To verify it, we analyze the statistics of the generated dataset to see the preferred positions of the classes. We calculate the averaged center points for the bounding boxes of five classes across over 20000\*25 images and plot these averaged center points in Fig 7. As shown, stop signs tend to appear in higher positions, while handbags favor lower positions. Another finding is that these objects do not exhibit a positional bias horizontally, clustering near the 256 dashed baseline.

## 4 WHAT CONTRIBUTES TO THE FORMATION OF TRIGGER PATCHES

In this part, we propose a potential explanation for the existence of trigger patches. While previous work Guo et al. (2024); Sun et al. (2024); Zheng et al. (2023) mainly focuses on the cross-attention maps and analyzes the interactions between specific noise, prompts, and models, we hypothesize that **these trigger patches are typical outliers in the sampled noise**, and have minimal correlation with prompts. Furthermore, we propose a method to synthesize trigger patches with great success.

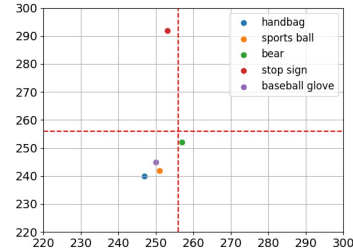


Figure 7: We plot the averaged center points for the bounding boxes of five classes. As the image size is  $512 \times 512$ , we marked the centered baseline of 256 with a red dashed line. The variance of these central points is greater on the vertical axis.

324 4.1 TWO-SAMPLE TEST  
325

326 An energy-based two-sample test measures the distance between the distributions of two samples by  
 327 computing the sum of pairwise Euclidean distances among all sample points (Székely & Rizzo, 2013).  
 328 Meanwhile, the test includes  $p$ -value to statistically quantify the extent to which the distributions's  
 329 difference. A low  $p$ -value (typically less than 0.05) suggests that the two sets of samples are not  
 330 subjected to the same distribution. Please refer to the Appendix E for detailed mechanism and the  
 331 python code we use for the 2-sample test. To construct a trigger patch group, we select 2,000 noises,  
 332 compute the center point of each bounding box, and extract  $24 \times 24$  trigger patches around the center.  
 333 We then create a negative group by randomly selecting 2,000 patches of  $24 \times 24$  in the same noises.  
 334 Additionally, we randomly select another group of patches of the same size to serve as a control group.  
 335 **The results show that the  $p$ -value between the trigger patch group and the negative groups**  
 336 **are 0.0, while the  $p$ -value between the negative group and the control group is 0.938.** Hence,  
 337 the trigger patches and those random patches in the negative groups are from different distributions.  
 338 Furthermore, we also find a clear negative correlation between the trigger entropy and the energy  
 339 distance. Please refer to the Appendix E.3 for more details.

340 4.2 HAND-CRAFTED TRIGGER PATCHES  
341

342 If the trigger patches are indeed outliers, it may be feasible to construct certain noises that deviate  
 343 from a normal Gaussian distribution to serve as artificially created trigger patches. To this end, we  
 344 conduct experiments to test various artificial trigger patches.

- 345 • Natural trigger patches: We extract the trigger patches with the lowest trigger entropy from  
 346 the 20,000 noise samples.
- 347 • Resampling baseline: We resample Gaussian noise maintaining the same mean and variance  
 348 to establish a baseline.
- 349 • Random baseline: We randomly select 25 sets, each consisting of four numbers, from a range  
 350 of 512. These numbers are interpreted as the coordinates for the final detected bounding  
 351 boxes, upon which we compute entropy. This baseline is designed to simulate scenarios  
 352 where each patch has an equal probability of generating an object.
- 353 • Shifted Gaussian: We sample Gaussian noises with altered standard deviation (std) so the  
 354 resultant noise follows a different Gaussian from the diffusion models' default noises.
- 355 • Sine Function: We create sinusoidal noise patches by firstly using a function that applies a  
 356 sine transformation to each coordinate axis ( $x, y, z$ ) and then summing up the values. We  
 357 then add them to an initial noise via interpolation as follows,

$$358 \overline{P_{(x,y,z)}} = \sin(\theta) \cdot \left[ \sin\left(\frac{2\pi x}{l_x}\right) + \sin\left(\frac{2\pi y}{l_y}\right) + \sin\left(\frac{2\pi z}{l_z}\right) \right] + \cos(\theta) \cdot P_{(x,y,z)}, \quad (2)$$

361 where  $P_{(x,y,z)}$  is the pixel value of the original patch at position  $(x, y, z)$ ,  $l_x$ ,  $l_y$  and  $l_z$  are  
 362 the widths of the trigger patch, and  $\theta$  is the interpolation parameter. In our case,  $l_x$ ,  $l_y$  and  $l_z$   
 363 are 24, 24 and 4, respectively.

364 The results are displayed in Table 4. Natural trigger patches achieved a success rate of 44.5%, which  
 365 exceeds the rates of randomly selected bounding boxes and the resampling of the region by 42.5%  
 366 and 36.0%, respectively. Notably, Sin Function patches yield comparable results when moderate  
 367 interpolation parameters are set, achieving an ISR of 49%. When the interpolation parameter  $\theta$  is  
 368 set at  $0.15 \cdot \frac{\pi}{2}$ , it achieves a significantly high ISR of 81.0%. However, this setting also causes image  
 369 distortion. Meanwhile, sampling Gaussian noise with a larger standard deviation appears to be more  
 370 effective in inducing trigger patches than using a smaller one, verifying that these trigger patches  
 371 might be considered outliers.

372 5 APPLICATIONS  
373

374 The ability to detect trigger patches enhances control over object locations in generated images,  
 375 opening the door to numerous applications. Here, we demonstrate two such applications: 1) In  
 376 scenarios where the prompt does not have positional information, we aim to increase the positional  
 377 diversity of the generated images. 2) Conversely, when the prompt includes explicit positional  
 378 guidance, our goal is to ensure that the generated images follow the provided directions. It is

378  
 379 Table 4: Main results on the injection experiments. The higher the ISR, the more effective the patch.  
 380 The left major column shows the ISRs for the baseline methods: Random, Resampling, and Natural.  
 381 The middle major column shows the results for the shifted Gaussian method with different standard  
 382 deviations(STD). The right major column shows the results for the Sine Function with different  
 383 interpolation weights.

	Baselines		Shifted Gaussian		Sine Function	
	ISR(%)	STD	ISR(%)	$\theta(\cdot \frac{\pi}{2})$	ISR(%)	
Random	1.0	0.8	8.5	0.08	33.5	
Resampling	8.5	1.2	29.0	0.10	49.0	
Natural	44.5	1.5	90.0	0.15	81.0	

390  
 391 important to note that manipulating trigger patches alone may not deliver state-of-the-art results. Our  
 392 main objective is to demonstrate that even such a straightforward approach can achieve reasonable  
 393 performance, highlighting the significant role that trigger patches play in the generation process.  
 394 Note that we use the detector obtained in Sec 3 to identify and manipulate trigger patches in both  
 395 applications, rather than relying on off-the-shelf trigger patches obtained through posterior methods.  
 396 **This demonstrates the open-vocabulary capability of our approach.**

### 398 5.1 ENHANCED LOCATION DIVERSITY BY REMOVING TRIGGER PATCHES

399 **Background** Researchers have observed various biases in diffusion models, including gender  
 400 bias (Luccioni et al., 2024) and color bias (Orgad et al., 2023). However, position bias, which is the  
 401 tendency for objects to consistently appear in the same locations across different generations, has  
 402 received minimal attention. This type of bias has significant implications, particularly in synthetic  
 403 data generation using diffusion models. For instance, when generating an automobile dataset, a  
 404 model exhibiting position bias might consistently place roadblocks in the left-bottom corner of the  
 405 image, leading to skewed data. Moreover, such a bias can affect the diversity of generated images in  
 406 applications like ChatGPT, where similar images are generated for varied prompts due to the presence  
 407 of trigger patches in the initial noise.

408 **Method** To mitigate this, we have developed a method involving the use of the detector for reject  
 409 sampling. This process begins with the detection of trigger patches in the initial noise. If the  
 410 confidence scores of the bounding boxes exceed a predefined threshold, the region within the box is  
 411 flagged for regeneration. Our approach is designed to ensure that the noise used for generation is  
 412 “pure” and has no strong trigger patches that could confine object placement. Please refer to Fig 11  
 413 for more visualized illustrations.

414 **Baselines** Although researchers have studied the positional bias in GAN-based generative mod-  
 415 els (Choi et al., 2021), no counterpart works have been found on the diffusion models. Here are the  
 416 baselines: Initno: focusing on the role of initial noise, Initno (Guo et al., 2024) may be the most  
 417 related one, though it needs the specific prompt for each generation process to take effect. Control:  
 418 we establish a Control group by generating images using standard methods without reject-sampling.  
 419 Random: we select Random bounding boxes of size  $24 \times 24$  from the initial noise. This approach  
 420 simulates a scenario where all pixels have an equal probability of generating an object, which is our  
 421 target. Attend (Chefer et al., 2023): we utilize the *StableDiffusionAttendAndExcitePipeline* class  
 422 from diffusers (von Platen et al., 2022) repository. We select the token IDs corresponding to the most  
 423 relevant words. For example, for the prompt “a ball on the left”, we configure the token IDs as “2,5”,  
 424 which correspond to the words “ball” and “left”. This ensures the model focuses on these specific  
 425 elements during image generation. Attention Refocusing Phung et al. (2024): we use the code from  
 426 the official repository. We use GPT-4 to generate layout bounding boxes. For each image, we prompt  
 427 the model to generate a new layout. Structured (Feng et al., 2022): we use the code from the official  
 428 repository and apply the default configurations in the README for the demos.

429 **Metrics and Configurations** We calculate the trigger entropy for the bounding boxes in these  
 430 groups to assess the impact of our method on diversity and positional bias. The entropy is calculated  
 431 as outlined in equation 1, with higher values indicating greater diversity. **The higher the Entropy is,**  
**the better.** Our experiment setup includes generating images from 10 random prompts described by  
 ChatGPT, followed by image generation using diffusion models. The objects’ bounding boxes are

432 identified using the same COCO detector in Sec 3, and entropy calculations are conducted on the  
 433 bounding boxes with confidence scores over 0.75. We set the rejection threshold for the confidence  
 434 score of the detector as 0.6 and conducted our experiments using 1000 different seeds. Note that the  
 435 prompts we use are in an open-vocabulary setting and include many objects beyond the five classes  
 436 used to train the detector. Please refer to the Appendix F.1 for the prompts we use and experiment  
 437 configurations.

439  
440 Table 5: Entropy values for different methods in location diversity.  
441

Methods	Control	Initno	Attend	Refocusing	Structured	Random	Ours
Entropy	135.97	139.89	145.16	102.097	133.92	170.64	<b>171.84</b>

444 As we can see from the table, images generated by our methods show great diversity in position,  
 445 with an entropy of 171.84, surpassing the control group by 31.95, very close to the pure random  
 446 outputs, which is 170.64. Meanwhile, Initno shows bad performance with an entropy of 139.89,  
 447 which is behind ours by a large margin. Other baselines also perform bad, which may result from the  
 448 fact that they are designed for setting a specific layout, not enhancing diversity. Please refer to the  
 449 Appendix F.1 for visualized results.

450 5.2 BETTER PROMPT FOLLOWING WITH TRIGGER PATCHES  
451

452 **Background and Methods** Research indicates that diffusion models often struggle to adhere to the  
 453 positional information specified in prompts. This issue is typically due to the appearance of trigger  
 454 patches in unintended locations as shown in the trigger-prompt interaction experiment in Sec 3.2.  
 455 For instance, a prominent trigger patch on the left side of an image can conflict with a prompt like  
 456 “a dog on the left”, resulting in generation failures. To address this, we propose a reject-sampling  
 457 technique to obtain an optimal initial noise where trigger patches align with the prompt requirements  
 458 even before generation. Specifically, we continue to resample noises until the center point of the  
 459 bounding box, which scores highest according to our detector, is positioned within the area targeted  
 460 by the prompt.

461 **Prompts** To assess our method’s effectiveness, we design 10 prompts incorporating the words **right**  
 462 or **left** and generate 500 images for each prompt. Please refer to Appendix F.2 for more details about  
 463 the prompts we used.

464 **Metrics** We generated images using 10 prompts that incorporate the words “right” or “left”,  
 465 eg, “a sports ball in the left”. We then used a pre-trained COCO detector from MMDetection to  
 466 verify whether the objects were correctly positioned according to the prompt. Supposing the x-axis  
 467 coordinates of the left and the right edges of the bounding boxes are  $x_1$  and  $x_2$  respectively, and  
 468 the image has a size of  $512 \times 512$ , we define *the generated object in the left part of the image* as  

$$\frac{x_1+x_2}{2} < \frac{512}{2}$$
. If *the generated object in the left part of the image* and the prompt specifies “left”, we  
 469 consider it a successful case. We calculate the GSR as the ratio of the number of successful cases to  
 470 the total number of cases. The higher the GSR is, the more effective the method.

471  
472 **Results** As seen in Table 6, our method, relying solely on the initial noise, achieves an impressive  
 473 guidance success rate (GSR) of 83.64%. While it is slightly surpassed by Attention Refocusing,  
 474 it offers substantial advantages in terms of simplicity and efficiency. **Our approach requires no  
 475 knowledge of the model or prompts and does not rely on access to a large language model.**  
 476 Moreover, using an NVIDIA RTX A6000, our method generates an image in approximately 5 seconds,  
 477 whereas Attention Refocusing takes around 15 seconds. Our method introduces a novel approach  
 478 to controllable generation by utilizing trigger patches even before the diffusion generation process,  
 479 providing an alternative to the traditional practice of manipulating cross-attention maps through  
 480 analysis. Please refer to Appendix F.2 for more visualization results.

481  
482 Table 6: Prompt following Results  
483

Methods	Control	Random	Attend	Attention Refocusing	Structured	Ours
GSR(%)	57.08	61.08	64.52	89.83	77.41	<b>83.64</b>

## 486 6 RELATED WORK

488 **Initial noise** In DDIM (Song et al., 2020), the final image is determined by the model parameters, the  
 489 text prompt, and the initial noise. While the model parameters and text prompts have been extensively  
 490 researched, the initial noise remains relatively under-explored. Mao et al. (2023) first highlights that  
 491 initial noises exhibit distinct preferences for certain layouts and analyze this phenomenon through the  
 492 lens of cross-attention. Sun et al. (2024) utilized an inverted reference image with finite inversion  
 493 steps to incorporate valuable spatial awareness, leading to a new framework for controllable image  
 494 generation. Guo et al. (2024) attributed failed generation cases to “bad initial noise” and proposed  
 495 optimizing the initial noise via cross-attention to achieve better results. On the other hand, Lin et al.  
 496 (2024) claim that common schedulers do not have zero terminal SNR at the final timestep, which  
 497 fails to reflect the reality that the model is given pure noise at inference, creating a gap between the  
 498 training and inference stages. In contrast, our claim is that the initial pure noise is not entirely “pure”  
 499 and contains specific trigger patches that can induce object generation during the inference stage.

500 Building on these studies, our research focuses on the role of initial noise. Unlike previous works  
 501 that qualitatively suggest the presence of positional information in initial noise, we provide evidence  
 502 for the **existence of trigger patches that tend to generate specific objects** by defining a metric to  
 503 quantitatively assess the effectiveness of these patches. Based on the findings above, we managed  
 504 to train a detector, which can detect trigger patches even before the image generation process.  
 505 Additionally, we propose that these trigger patches are universal and capable of generalizing across  
 506 different positions, prompts, and background noises. While prior research primarily examines noise  
 507 from a cross-attention perspective, we discover that the intriguing properties might stem from **the**  
 508 **statistical characteristics of these patches**, which are outliers within the initial noise. We identify  
 509 significant applications in enhancing positional diversity. While previous studies mainly addressed  
 510 biases related to gender, color, and texture, our findings reveal that noise with strong trigger patches  
 511 can introduce positional bias. Finally, in applications, previous methods require performing diffusion  
 512 steps and accessing cross-attention maps. In contrast, our approach does not rely on any knowledge  
 513 of the prompt or the model. Simply applying the detector to the noise is sufficient to anticipate the  
 514 position of the generated object.

515 **Types of objection detection** Object detection is a fundamental computer vision technique that  
 516 identifies and locates objects in digital images and videos. Various detection networks have been devel-  
 517 oped for different application scenarios, such as static images (Ren et al., 2015), video frames (Wojke  
 518 et al., 2017), depth images (Reading et al., 2021), point clouds (Qi et al., 2017), sequential data (Lea  
 519 et al., 2017), and multi-channel images (Chen et al., 2016). However, we propose a novel and  
 520 counter-intuitive approach: using **pure Gaussian noise** as the input, the model is trained to learn  
 521 from these noises and extract patches with intriguing properties. To the best of our knowledge, this is  
 522 the first study to propose such an approach.

## 523 7 CONCLUSION

524 In this study, we have uncovered specific trigger patches within the initial noise that are likely to  
 525 induce object generation. We subsequently developed a detector capable of identifying these trigger  
 526 patches from the initial noise prior to the generation process. We characterized these trigger patches  
 527 as outliers within Gaussian noise and conducted experiments to validate this classification. Finally,  
 528 we show two potential applications for our detector, both of which have demonstrated excellent  
 529 performance. We leave more applications for future work.

## 530 8 LIMITATIONS

531 One limitation is the size of the dataset we used for training the trigger patch detector. Due to limited  
 532 computational resources, we only train on 20,000 noises and 500,000 images, so the performance  
 533 of our detector can be potentially improved with a larger training set. Also, this work is the first to  
 534 demonstrate the existence of trigger patches, so there are many potential applications that have not  
 535 been explored in the current paper.

## 536 537 REFERENCES

538 Yogesh Balaji, Seungjun Nah, Xun Huang, Arash Vahdat, Jiaming Song, Qinsheng Zhang, Karsten  
 539 Kreis, Miika Aittala, Timo Aila, Samuli Laine, et al. ediff-i: Text-to-image diffusion models with

- 540        an ensemble of expert denoisers. *arXiv preprint arXiv:2211.01324*, 2022.  
 541
- 542        Hila Chefer, Yuval Alaluf, Yael Vinker, Lior Wolf, and Daniel Cohen-Or. Attend-and-excite:  
 543        Attention-based semantic guidance for text-to-image diffusion models. *ACM Transactions on  
 544        Graphics (TOG)*, 42(4):1–10, 2023.
- 545        Kai Chen, Jiaqi Wang, Jiangmiao Pang, Yuhang Cao, Yu Xiong, Xiaoxiao Li, Shuyang Sun, Wansen  
 546        Feng, Ziwei Liu, Jiarui Xu, et al. Mmdetection: Open mmlab detection toolbox and benchmark.  
 547        *arXiv preprint arXiv:1906.07155*, 2019.
- 548        Yushi Chen, Hanlu Jiang, Chunyang Li, Xiuping Jia, and Pedram Ghamisi. Deep feature extrac-  
 549        tion and classification of hyperspectral images based on convolutional neural networks. *IEEE  
 550        transactions on geoscience and remote sensing*, 54(10):6232–6251, 2016.
- 551        Jooyoung Choi, Jungbeom Lee, Yonghyun Jeong, and Sungroh Yoon. Toward spatially unbiased  
 552        generative models. *arXiv preprint arXiv:2108.01285*, 2021.
- 553
- 554        Prafulla Dhariwal and Alexander Nichol. Diffusion models beat gans on image synthesis. *Advances  
 555        in neural information processing systems*, 34:8780–8794, 2021.
- 556
- 557        Patrick Esser, Sumith Kulal, Andreas Blattmann, Rahim Entezari, Jonas Müller, Harry Saini, Yam  
 558        Levi, Dominik Lorenz, Axel Sauer, Frederic Boesel, et al. Scaling rectified flow transformers for  
 559        high-resolution image synthesis. In *Forty-first International Conference on Machine Learning*,  
 560        2024.
- 561        Weixi Feng, Xuehai He, Tsu-Jui Fu, Varun Jampani, Arjun Akula, Pradyumna Narayana, Sugato  
 562        Basu, Xin Eric Wang, and William Yang Wang. Training-free structured diffusion guidance for  
 563        compositional text-to-image synthesis. *arXiv preprint arXiv:2212.05032*, 2022.
- 564
- 565        Xiefan Guo, Jinlin Liu, Miaomiao Cui, Jiankai Li, Hongyu Yang, and Di Huang. Initno: Boosting  
 566        text-to-image diffusion models via initial noise optimization. *arXiv preprint arXiv:2404.04650*,  
 567        2024.
- 568
- 569        Kaiming He, Xiangyu Zhang, Shaoqing Ren, and Jian Sun. Deep residual learning for image  
 570        recognition. In *Proceedings of the IEEE conference on computer vision and pattern recognition*,  
 pp. 770–778, 2016.
- 571
- 572        Amir Hertz, Ron Mokady, Jay Tenenbaum, Kfir Aberman, Yael Pritch, and Daniel Cohen-Or. Prompt-  
 573        to-prompt image editing with cross attention control. *arXiv preprint arXiv:2208.01626*, 2022.
- 574
- 575        Jonathan Ho and Tim Salimans. Classifier-free diffusion guidance. *arXiv preprint arXiv:2207.12598*,  
 2022.
- 576
- 577        Jonathan Ho, Ajay Jain, and Pieter Abbeel. Denoising diffusion probabilistic models. *Advances in  
 578        neural information processing systems*, 33:6840–6851, 2020.
- 579
- 580        Tero Karras, Miika Aittala, Timo Aila, and Samuli Laine. Elucidating the design space of diffusion-  
 581        based generative models. *Advances in neural information processing systems*, 35:26565–26577,  
 2022.
- 582
- 583        Yuval Kirstain, Adam Polyak, Uriel Singer, Shahbuland Matiana, Joe Penna, and Omer Levy. Pick-  
 584        a-pic: An open dataset of user preferences for text-to-image generation. *Advances in Neural  
 Information Processing Systems*, 36:36652–36663, 2023.
- 585
- 586        Colin Lea, Michael D Flynn, Rene Vidal, Austin Reiter, and Gregory D Hager. Temporal convolutional  
 587        networks for action segmentation and detection. In *proceedings of the IEEE Conference on  
 Computer Vision and Pattern Recognition*, pp. 156–165, 2017.
- 588
- 589        Xiang Li, Wenhui Wang, Lijun Wu, Shuo Chen, Xiaolin Hu, Jun Li, Jinhui Tang, and Jian Yang. Gen-  
 590        eralized focal loss: Learning qualified and distributed bounding boxes for dense object detection.  
 591        *Advances in Neural Information Processing Systems*, 33:21002–21012, 2020.
- 592
- 593        Yumeng Li, Margret Keuper, Dan Zhang, and Anna Khoreva. Divide & bind your attention for  
 improved generative semantic nursing. In *34th British Machine Vision Conference 2023, BMVC  
 2023*, 2023.

- 594 Shanchuan Lin, Bingchen Liu, Jiashi Li, and Xiao Yang. Common diffusion noise schedules and  
 595 sample steps are flawed. In *Proceedings of the IEEE/CVF winter conference on applications of*  
 596 *computer vision*, pp. 5404–5411, 2024.
- 597 Tsung-Yi Lin, Michael Maire, Serge Belongie, James Hays, Pietro Perona, Deva Ramanan, Piotr  
 598 Dollár, and C Lawrence Zitnick. Microsoft coco: Common objects in context. In *Computer Vision–*  
 599 *ECCV 2014: 13th European Conference, Zurich, Switzerland, September 6–12, 2014, Proceedings,*  
 600 *Part V 13*, pp. 740–755. Springer, 2014.
- 601 Luping Liu, Yi Ren, Zhijie Lin, and Zhou Zhao. Pseudo numerical methods for diffusion models on  
 602 manifolds. *arXiv preprint arXiv:2202.09778*, 2022a.
- 603 Nan Liu, Shuang Li, Yilun Du, Antonio Torralba, and Joshua B Tenenbaum. Compositional visual  
 604 generation with composable diffusion models. In *European Conference on Computer Vision*, pp.  
 605 423–439. Springer, 2022b.
- 606 Cheng Lu, Yuhao Zhou, Fan Bao, Jianfei Chen, Chongxuan Li, and Jun Zhu. Dpm-solver: A fast  
 607 ode solver for diffusion probabilistic model sampling in around 10 steps. *Advances in Neural*  
 608 *Information Processing Systems*, 35:5775–5787, 2022.
- 609 Sasha Luccioni, Christopher Akiki, Margaret Mitchell, and Yacine Jernite. Stable bias: Evaluating  
 610 societal representations in diffusion models. *Advances in Neural Information Processing Systems*,  
 611 36, 2024.
- 612 Chengqi Lyu, Wenwei Zhang, Haian Huang, Yue Zhou, Yudong Wang, Yanyi Liu, Shilong Zhang,  
 613 and Kai Chen. Rtdet: An empirical study of designing real-time object detectors. *arXiv preprint*  
 614 *arXiv:2212.07784*, 2022.
- 615 Jiafeng Mao, Xuetong Wang, and Kiyoharu Aizawa. Guided image synthesis via initial image editing  
 616 in diffusion model. In *Proceedings of the 31st ACM International Conference on Multimedia*, pp.  
 617 5321–5329, 2023.
- 618 Alex Nichol, Prafulla Dhariwal, Aditya Ramesh, Pranav Shyam, Pamela Mishkin, Bob McGrew,  
 619 Ilya Sutskever, and Mark Chen. Glide: Towards photorealistic image generation and editing with  
 620 text-guided diffusion models. *arXiv preprint arXiv:2112.10741*, 2021.
- 621 Hadas Orgad, Bahjat Kawar, and Yonatan Belinkov. Editing implicit assumptions in text-to-image  
 622 diffusion models. In *Proceedings of the IEEE/CVF International Conference on Computer Vision*,  
 623 pp. 7053–7061, 2023.
- 624 Quynh Phung, Songwei Ge, and Jia-Bin Huang. Grounded text-to-image synthesis with attention refo-  
 625 cusing. In *Proceedings of the IEEE/CVF Conference on Computer Vision and Pattern Recognition*,  
 626 pp. 7932–7942, 2024.
- 627 Dustin Podell, Zion English, Kyle Lacey, Andreas Blattmann, Tim Dockhorn, Jonas Müller, Joe  
 628 Penna, and Robin Rombach. Sdxl: Improving latent diffusion models for high-resolution image  
 629 synthesis. *arXiv preprint arXiv:2307.01952*, 2023.
- 630 Charles R Qi, Hao Su, Kaichun Mo, and Leonidas J Guibas. Pointnet: Deep learning on point sets  
 631 for 3d classification and segmentation. In *Proceedings of the IEEE conference on computer vision*  
 632 and pattern recognition, pp. 652–660, 2017.
- 633 Cody Reading, Ali Harakeh, Julia Chae, and Steven L Waslander. Categorical depth distribution  
 634 network for monocular 3d object detection. In *Proceedings of the IEEE/CVF Conference on*  
 635 *Computer Vision and Pattern Recognition*, pp. 8555–8564, 2021.
- 636 Shaoqing Ren, Kaiming He, Ross Girshick, and Jian Sun. Faster r-cnn: Towards real-time object  
 637 detection with region proposal networks. *Advances in neural information processing systems*, 28,  
 638 2015.
- 639 Robin Rombach, Andreas Blattmann, Dominik Lorenz, Patrick Esser, and Björn Ommer. High-  
 640 resolution image synthesis with latent diffusion models. In *Proceedings of the IEEE/CVF confer-*  
 641 *ence on computer vision and pattern recognition*, pp. 10684–10695, 2022.

- 648 Chitwan Saharia, William Chan, Saurabh Saxena, Lala Li, Jay Whang, Emily L Denton, Kamyar  
 649 Ghasemipour, Raphael Gontijo Lopes, Burcu Karagol Ayan, Tim Salimans, et al. Photorealistic  
 650 text-to-image diffusion models with deep language understanding. *Advances in Neural Information  
 651 Processing Systems*, 35:36479–36494, 2022.
- 652 Jiaming Song, Chenlin Meng, and Stefano Ermon. Denoising diffusion implicit models. *arXiv  
 653 preprint arXiv:2010.02502*, 2020.
- 654 Wenqiang Sun, Teng Li, Zehong Lin, and Jun Zhang. Spatial-aware latent initialization for control-  
 655 lable image generation. *arXiv preprint arXiv:2401.16157*, 2024.
- 656 Gábor J Székely and Maria L Rizzo. Energy statistics: A class of statistics based on distances.  
 657 *Journal of statistical planning and inference*, 143(8):1249–1272, 2013.
- 658 Patrick von Platen, Suraj Patil, Anton Lozhkov, Pedro Cuenca, Nathan Lambert, Kashif Rasul,  
 659 Mishig Davaadorj, Dhruv Nair, Sayak Paul, William Berman, Yiyi Xu, Steven Liu, and Thomas  
 660 Wolf. Diffusers: State-of-the-art diffusion models. [https://github.com/huggingface/  
 661 diffusers](https://github.com/huggingface/diffusers), 2022.
- 662 Andrey Voynov, Kfir Aberman, and Daniel Cohen-Or. Sketch-guided text-to-image diffusion models.  
 663 In *ACM SIGGRAPH 2023 Conference Proceedings*, pp. 1–11, 2023.
- 664 Zijie J Wang, Evan Montoya, David Munechika, Haoyang Yang, Benjamin Hoover, and Duen Horng  
 665 Chau. Diffusiondb: A large-scale prompt gallery dataset for text-to-image generative models.  
 666 *arXiv preprint arXiv:2210.14896*, 2022.
- 667 Nicolai Wojke, Alex Bewley, and Dietrich Paulus. Simple online and realtime tracking with a  
 668 deep association metric. In *2017 IEEE international conference on image processing (ICIP)*, pp.  
 669 3645–3649. IEEE, 2017.
- 670 Lvmin Zhang, Anyi Rao, and Maneesh Agrawala. Adding conditional control to text-to-image  
 671 diffusion models. In *Proceedings of the IEEE/CVF International Conference on Computer Vision*,  
 672 pp. 3836–3847, 2023.
- 673 Guangcong Zheng, Xianpan Zhou, Xuewei Li, Zhongang Qi, Ying Shan, and Xi Li. Layoutdiffusion:  
 674 Controllable diffusion model for layout-to-image generation. In *Proceedings of the IEEE/CVF  
 675 Conference on Computer Vision and Pattern Recognition*, pp. 22490–22499, 2023.
- 676 Zhenyu Zhou, Defang Chen, Can Wang, Chun Chen, and Siwei Lyu. Simple and fast distillation of  
 677 diffusion models. *arXiv preprint arXiv:2409.19681*, 2024.

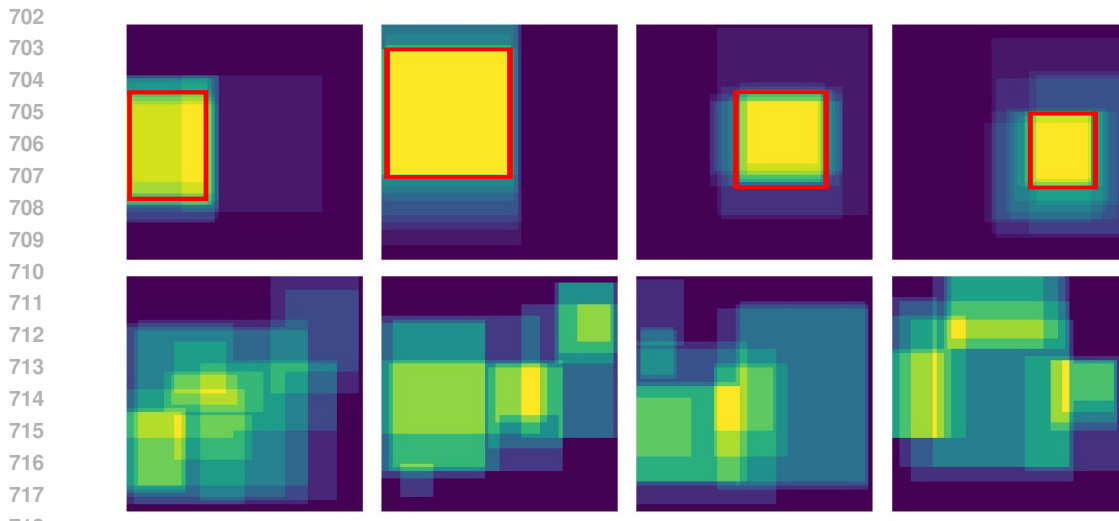
## 684 A VISUALIZATION

## 687 B DATASET CREATION

689 **Prompts** We use ChatGPT to generate sentences based on the given object name. The prompt is as  
 690 follows:

692 **Prompt**

693     ## Task:  
 694       Generate a sentence describing a scene that includes the given object, ensuring no additional  
 695       objects are mentioned.  
 696     ## Example:  
 697       Input: sports ball  
 698       Output: A sports ball is caught in a fence.  
 699     ## Task:  
 700       I will give you 5 kinds of objects, 'sports ball', 'baseball glove', 'bear', 'handbag', 'stop sign'.  
 701       Please generate 5 sentences for each object.



724  
725  
726  
727 **Generated Sentences** The final prompts for the five objects are as follows:  
728  
729  
730  
731

### Sports Ball

- 732 1. A sports ball is caught in a fence.
- 733 2. A sports ball lies forgotten under a tree.
- 734 3. A sports ball sits on a sandy beach.
- 735 4. A sports ball rests on a grassy land.
- 736 5. A sports ball stands out on a muddy field.

### Baseball Glove

- 740 1. The baseball glove waits by the fence.
- 741 2. A young athlete breaks in a new baseball glove.
- 742 3. A baseball glove rests on the dugout bench.
- 743 4. His baseball glove hangs by the door.
- 744 5. A baseball glove is left on the fence during practice.

### Bear

- 749 1. A grizzly bear fishes in a rushing river.
- 750 2. A bear cub explores the forest with curiosity.
- 751 3. A bear catches a fish in the river.
- 752 4. A black bear forages for berries in the woods.
- 753 5. A bear sniffs the forest floor.

756

**Handbag**

757

- 758 1. A fashionable handbag complements an elegant outfit.
- 759 2. A woman carries a stylish handbag on her shoulder.
- 760 3. A handbag rests on a cafe table during lunch.
- 761 4. A handbag holds essentials for a day of shopping.
- 762 5. A handbag adds a pop of color to a monochrome look.

763

764

**Stop Sign**

765

- 766 1. A red stop sign halts traffic at an intersection.
- 767 2. A stop sign stands alone on a country road.
- 768 3. A stop sign is covered in a layer of snow.
- 769 4. A stop sign is adorned with event flyers.
- 770 5. A stop sign stands at the entrance to a neighborhood.

771

772

**Image generating** We adopt the Stable Diffusion V2 Rombach et al. (2022) from diffusers von Platen et al. (2022) to generate images. On an NVIDIA 2080TI GPU, generating a single image takes approximately 12 seconds. In total, producing 500k images on an 8-GPU machine takes around 7 days.

773

774

775

776

777

778

779

780

781

782

783

**Detector** We adopt RTMDet Lyu et al. (2022) from the MMDetection repo Chen et al. (2019) for its efficiency and good accuracy. During inference, we observed that multiple bounding boxes are often proposed for a single image. For the annotations detected by the COCO detector, we retain only those with a confidence score above 0.75, and where the predicted class matches the given prompt.

## C GENERALIZATION

784

785

786

787

788

789

790

791

792

In this section, we conduct a series of ablation experiments to verify the trigger patches are “universal” and can take effect across different settings. We verified the effectiveness of the trigger patches by following the protocol of the **Generalization paragraph** described in Sec 3.2. Specifically, we injected the trigger patches into different random noise samples and used the blended noise to generate images. We then determined the success of the injection by checking whether the targeted region generated the intended object. A successful injection is defined as a detected bounding box occupying more than 75 percent of the trigger patch region. The Injection Success Rate (ISR) is calculated as the ratio of successful injections to the total number of cases, with **a higher ISR indicating a more obvious trigger patch phenomenon**.

793

794

### C.1 GENERALIZATION RESULTS FOR DIFFERENT SAMPLING CONFIGURATIONS

795

796

797

In this subsection, we evaluate whether the trigger patch generalizes effectively across different sampling steps, aspect ratios, and schedulers.

798

799

800

801

802

803

We conduct experiments using Stable Diffusion v2 provided by Diffusers von Platen et al. (2022). The default configuration is set to 50 timesteps, a PNDM Liu et al. (2022a) scheduler, and an 1:1 aspect ratio. For each configuration, we also conducted a resampling baseline, where Gaussian noise was resampled within the target patch while maintaining the same mean and variance. **A significant gap between the experimental group and the baseline indicates the effectiveness of the trigger patch in those settings.** The higher the GAP is, the more effective it is. The results are as follows:

804

805

806

807

808

809

Table 7: Generalization Results for Different Time Steps.

Time Steps	30	40	50	60
Resampling Baseline	0.100	0.085	0.105	0.090
Experimental Group	0.645	0.665	0.660	0.630
Gap	0.545	0.580	0.555	0.540

Table 8: Generalization Results for Different Deterministic and Stochastic Schedulers.

Deterministic Schedulers				
Schedulers	Resampling Baseline	Experimental Group	Gap	
PNDM Liu et al. (2022a)	0.105	0.660	0.555	
LMSD Karras et al. (2022)	0.095	0.620	0.525	
EulerDiscrete Karras et al. (2022)	0.115	0.620	0.505	
HeunDiscrete Karras et al. (2022)	0.110	0.610	0.500	
DDIM Song et al. (2020)	0.145	0.630	0.485	

Stochastic Schedulers				
Schedulers	Resampling Baseline	Experimental Group	Gap	
DPM Lu et al. (2022)	0.180	0.690	0.510	
KDPM Karras et al. (2022)	0.240	0.405	0.165	
EulerAncestral Karras et al. (2022)	0.180	0.165	-0.015	
TCDScheduler Zhou et al. (2024)	0.105	0.650	0.545	
DDPM Ho et al. (2020)	0.145	0.155	0.010	

Table 9: Generalization Results for different Aspect Ratios.

Aspect Ratios	16:9	4:3	1:1	3:4	9:16
Resampling Baseline	0.030	0.090	0.105	0.050	0.030
Experimental Group	0.440	0.630	0.660	0.475	0.500
Gap	0.410	0.540	0.555	0.425	0.470

In the three tables, an obvious gap can be observed between the Resampling baseline and the Experiment Group, showing that our trigger patch can induce the generation of the object successfully across different sampling configurations. As observed from the Tab 8, our method underperforms with certain stochastic samplers. The reason lies in the nature of stochastic samplers, which introduce noise to the latent variables at each diffusion step. If the added noise is large enough, it can overwrite the initial noise to some extent, diminishing the influence of our trigger patch. Conversely, if the introduced noise is small, our trigger patch is still able to exert a strong effect. To test this hypothesis, we conducted a series of experiments using the DDIM Song et al. (2020) sampler from the diffusers, which includes a parameter  $\eta$  to control the strength of the introduced noise: It has a parameter  $\eta$  which controls the strength of the introduced noise. Setting  $\eta = 0.0$  makes the sampler behave like a deterministic one. The suggested value for  $\eta$  is 0.1-0.3. In Tab 10, a negative correlation between  $\eta$  and the ISR Gap is observed. This suggests that the noise level directly impacts the trigger patch's ability to influence the diffusion process.

Table 10: Effect of eta Parameter in the DDIM Sampler on ISR Gap.

eta	Resampling Baseline	Experimental Group	Gap
0.0	0.145	0.630	0.485
0.01	0.140	0.620	0.480
0.05	0.180	0.635	0.455
0.1	0.165	0.640	0.475
0.2	0.145	0.555	0.410
0.5	0.160	0.355	0.195

## C.2 GENERALIZATION RESULTS OF DIFFERENT MODELS

In this subsection, we evaluate whether the trigger patch generalizes well across different models. We selected three types of models and adopted the same approach as described in the previous subsection.

1. **SOTA T2I models:** We selected Stable Diffusion XL Podell et al. (2023).

- 864  
 865    2. **Finetuned models:** We used the off-the-shelf model “oraul/finetuned\_stable-diffusion-v1-  
 866    4\_FFHQ\_smaller\_ep\_2” from the Hugging Face Hub.  
 867  
 868    3. **LoRA models:** Most LoRA models often overfit certain objects and show degraded per-  
 869    formance. Therefore, we used style-LoRA models that focus on altering the style of  
 870    the model output. Specifically, we employed two adapters from Hugging Face: Water  
 871    Color (available at “ostris/watercolor\_style\_lora\_sdxl”) and Crayons (available at “os-  
 872    tris/crayon\_style\_lora\_sdxl”).  
 873  
 874    4. **DiT models:** We adopted Stable Diffusion v3 Esser et al. (2024) with a **DiT** backbone. To  
 875    ensure compatibility, we modified the shape of the input latent to produce output images  
 876    of the same size as those generated by other Stable Diffusion models. For implementation,  
 877    we utilized the code from Hugging Face, using the model ID “stabilityai/stable-diffusion-3-  
 878    medium-diffusers”. This adaptation allowed us to integrate the unique architecture of the  
 879    DiT backbone while maintaining consistency in output dimensions for fair comparisons.

Table 11: Generalization Results of Different Models

Models	SDXL	Oraul	Lora Water Color	Lora Crayons	SD3
Resampling Baseline	0.355	0.330	0.265	0.305	<b>0.219</b>
Experimental Group	0.500	0.525	0.565	0.695	<b>0.441</b>
Gap	0.145	0.195	0.300	0.390	<b>0.222</b>

These results indicate that our method can generalize well across different models.

## D DETECTOR TRAINING

**Shuffled Data** We establish a **reasonable baseline** by permuting the annotations of different noises, which prevents the detector from receiving any meaningful information from the noise. Please refer to the Fig 9 for more details.

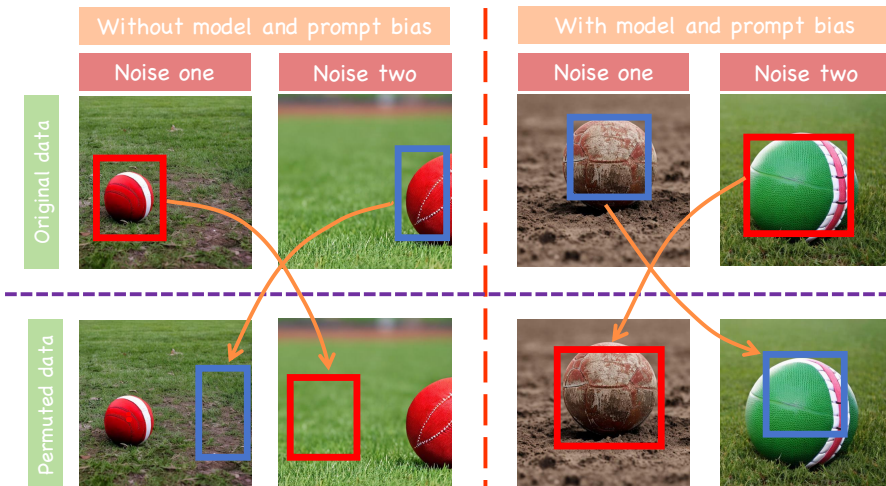


Figure 9: Shuffled Data: We shuffled the annotations associated with the noise samples. Initially, in the top row, Noise One was labeled with Annotation One, and Noise Two with Annotation Two. After permutation, shown in the bottom row, Noise One is now labeled with Annotation Two, and Noise Two with Annotation One. Ideally, in scenarios with a strong bias, permuting the annotations should have minimal or no impact on the final results. This is because, in both shuffled and unshuffled datasets, the bounding boxes remain centrally located within the image.

**Training** To train a detector capable of anticipating trigger patches, we utilize the MMDetection repository Chen et al. (2019). Our approach integrates Generalized Focal Loss Li et al. (2020) and a ResNet101 with a 4× width expansion He et al. (2016). We follow the COCO dataset configurations

918 provided by the repository. To handle noise with dimensions of  $4 \times 64 \times 64$ , we set the input  
 919 dimension to 4. During training, we observed that strong data augmentation techniques, such as  
 920 Flip and Random Resize, significantly impaired performance, leading us to eliminate them. The  
 921 training was conducted on four NVIDIA GTX 2080 Ti GPUs with 17.5k noise samples, and the  
 922 loss converged after 20 epochs. We report the mean Average Precision (mAP50) threshold on the 1k  
 923 validation dataset.

924  
 925 **Comparison with object detectors on COCO detector** Our method achieves a mAP<sub>50</sub> of 0.333,  
 926 while Faster R-CNN Ren et al. (2015) achieves a mAP<sub>50</sub> of 0.596 on COCO validation set Lin et al.  
 927 (2014).

928 However, due to the complexity of our task, direct comparisons with state-of-the-art detectors on  
 929 real-world images may not be reasonable. Here are the challenges for our task:  
 930

- 931 1. **Different Input Characteristics:** Our inputs are Gaussian noises, which differ significantly  
 932 from real-world images that have clear boundaries and semantic segments. Thus, a direct  
 933 comparison is meaningless. Meanwhile, we believe we are among the **first** to explore this  
 934 task in such a context. There is still a long way to go for our settings.
- 935 2. **Object Size Variation:** Our trigger patches are universal and **do not depend on specific  
 936 prompts**. However, we observed that object sizes vary greatly. For instance, in a  $512 \times 512$   
 937 image, the average area for a bear is 69,274 pixels, whereas for a sports ball, it is only 29,919  
 938 pixels. Despite this variation, our detector achieves comparable performance, demonstrating  
 939 its capability to accurately detect the **center points** of trigger patches even under these  
 940 challenging conditions.
- 941 3. **Challenges with Advanced Techniques:** We experimented with various configurations,  
 942 finding that most advanced techniques, which typically improve object detection, did not  
 943 benefit our task. Techniques like random cropping in data augmentation even reduced  
 944 performance, possibly due to the nature of our input data. As a result, we simplified our  
 945 training configuration to retain the statistical properties as much as possible.

946 Based on the reasons above, we establish a **reasonable baseline** by permuting the annotations of  
 947 different noises, which prevents the detector from receiving any meaningful information from the  
 948 noise. This baseline achieves an mAP50 of **0.201**, while our method achieves an mAP50 of **0.333**,  
 949 clearly highlighting the capacity of our detector. Additionally, our applications in Sec 5.1 and Sec 5.2  
 950 are all based on the detector we trained. The **successful application of our detector in Section 4**  
 951 further validates its effectiveness.

## 954 E ENERGY-BASED TWO-SAMPLE TEST

### 956 E.1 THE MECHANISM

958 First, the energy distance quantifies the distance between two probability distributions and computes  
 959 the energy distance between the two tested sets, named  $T_{\text{observed}}$ . Then, the two samples are combined  
 960 into one joint sample, which is randomly shuffled multiple times (e.g., 1000 times). After each  
 961 random permutation, the shuffled sample is split into two new samples. For each random permutation,  
 962 the statistic for the newly formed samples, denoted as  $T_{\text{permuted}}$ , is computed. The p-value for the  
 963 permutation test is calculated as:

$$965 \quad \text{p-value} = \frac{\text{Number of times } T_{\text{perm}} \geq T_{\text{obs}}}{\text{Total number of permutations}}$$

968 In our experiments, we find it extremely time-consuming to compute the energy distance, so we set  
 969 the sampling time to 1000. In this case, the p-value can be 0.0 if all  $T_{\text{perm}}$  values are smaller than  
 970  $T_{\text{observed}}$ . We believe that 1000 permutations are sufficient to ensure the p-value remains below 0.001,  
 971 which is considerably smaller than the conventional threshold of 0.05.

972 E.2 PYTHON CODE  
973974 Below is the Python code we used for the two-sample test:  
975

```

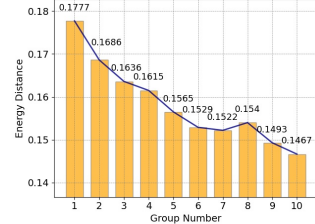
976
977 1 import numpy as np
978 2 from scipy.spatial.distance import cdist
979 3 from tqdm import tqdm
980 4
981 5 def energy_distance(x, y):
982 6     """Compute the energy distance between two datasets"""
983 7     x, y = np.asarray(x), np.asarray(y)
984 8     xy_distance = np.mean(cdist(x, y, 'euclidean'))
985 9     xx_distance = np.mean(cdist(x, x, 'euclidean'))
986 10    yy_distance = np.mean(cdist(y, y, 'euclidean'))
987 11    return 2 * xy_distance - xx_distance - yy_distance
988 12
989 13 def permutation_test(x, y, num_permutations=1000):
990 14     """Perform a permutation test to compute the p-value
991 15     for the energy distance"""
992 16     combined = np.vstack([x, y])
993 17     original_distance = energy_distance(x, y)
994 18     count = 0
995 19
996 20     for _ in tqdm(range(num_permutations)):
997 21         np.random.shuffle(combined) # Randomly shuffle the data
998 22         new_x = combined[:len(x)]
999 23         new_y = combined[len(x):]
1000 24         permuted_distance = energy_distance(new_x, new_y)
1001 25         if permuted_distance >= original_distance:
1002 26             count += 1
1003 27
1004 28     p_value = count / num_permutations
1005 29     return original_distance, p_value
1006

```

Listing 1: Two Sample Test Code

1007 E.3 A NEGATIVE CORRELATION BETWEEN THE TRIGGER ENTROPY AND THE DISTANCE  
1008 ENERGY  
1009

1010 To study the correlation between the trigger entropy and the distance  
1011 energy, we divide 20,000 noises into ten groups according to the  
1012 order of Trigger Entropy with 2,000 noises each and the first group  
1013 has the lowest Trigger Entropy. Then we compute the center point  
1014 of each bounding box, and extract a  $24 \times 24$  trigger patch around  
1015 the center. Following these steps, we obtain a list of trigger patches  
1016 for each group. We then create ten negative groups by randomly  
1017 selecting a patch of  $24 \times 24$  in the same noise. Additionally, we craft  
1018 a control group by randomly selecting patches of the same size. **The**  
1019 **results show that all the  $p$ -values between trigger patch groups** Figure 10: Energy Distance  
1020 **and negative groups are 0.0, while the  $p$ -value between the negative prompts and the control**  
1021 **group is 0.938.** Note that a  $p$ -value of 0.0 in our settings actually means that the true  $p$ -value is  
1022 under 0.001, detailed in the Appendix E. Hence, the trigger patches and those random patches in the  
1023 negative groups are from different distributions. Furthermore, we examine the relationship between  
1024 the energy distance of trigger patches from negative patches and the trigger entropy, as illustrated in  
1025 Figure 10. This figure reveals a clear negative correlation: the greater the deviation of a patch from  
the original distribution, the more likely it is to be a trigger patch characterized by low trigger entropy.  
This observation again supports our hypothesis that these trigger patches are outliers within the noise.



1026  
1027

## F APPLICATIONS

1028  
1029

### F.1 ENHANCED LOCATION DIVERSITY BY REMOVING TRIGGER PATCHES

1030  
1031  
1032

**Prompts** We prompt ChatGPT to generate sentences describing complex scenes to test the **open-vocabulary generation of our method**, besides the 5 coco classes. The prompts we use are as follows:

1033  
1034

#### Prompts for Location diversity

1035  
1036  
1037  
1038  
1039  
1040  
1041  
1042  
1043  
1044  
1045  
1046  
1047  
1048  
1049  
1050  
1051  
1052  
1053  
1054  
1055  
1056  
1057  
1058  
1059  
1060  
1061  
1062  
1063  
1064  
1065  
1066  
1067  
1068  
1069  
1070  
1071  
1072  
1073  
1074  
1075  
1076  
1077  
1078  
1079

1. The golden sunlight filters through the dense canopy of the forest, casting dappled shadows on the moss-covered ground.
2. A red bicycle leans against a gnarled oak tree, its wheels slightly caked with mud from the morning's ride.
3. Nearby, a picnic table is set with a checkered cloth, and atop it rests a basket filled with fresh fruit and sandwiches.
4. A frisbee lies forgotten on the grass, a few feet away from a sleeping dog with its fur glistening in the sun.
5. In the background, a kite dances in the sky, its bright colors a stark contrast against the blue expanse above.
6. A laptop is open on the table, displaying vibrant images of nature, momentarily abandoned for the allure of the outdoors.
7. A baseball glove and ball sit on the bench, remnants of a game played in the spirit of friendly competition.
8. A traffic cone marks the end of a nearby trail, signaling caution to the cyclists and hikers passing by.
9. A traffic cone marks the end of a nearby trail, signaling caution to the cyclists and hikers passing by.
10. As the day wanes, the street lights begin to flicker on, their glow adding a soft luminescence to the tranquil scene.

**Experiment settings** For each prompt and each method, we generate 1000 images. Please refer to Fig 11 for visualization results. We adopt an off-the-shelf detector Lyu et al. (2022) from the MMDection repo Chen et al. (2019) to detect the bounding box and calculate the average entropy. The higher the average entropy is, the better.

### F.2 BETTER PROMPT FOLLOWING APPLICATION BY INJECTING TRIGGER PATCHES

**Prompts** We designed 10 prompts with direct positional information to test the methods.

#### Prompts Targeted at Left

1. a sports ball in the left.
2. a cow in the left.
3. an apple in the left.
4. a bicycle in the left.
5. a vase in the left.

#### Prompts Targeted at Right

1. a sports ball in the right.
2. a cow in the right.
3. an apple in the right.
4. a bicycle in the right.
5. a vase in the right.

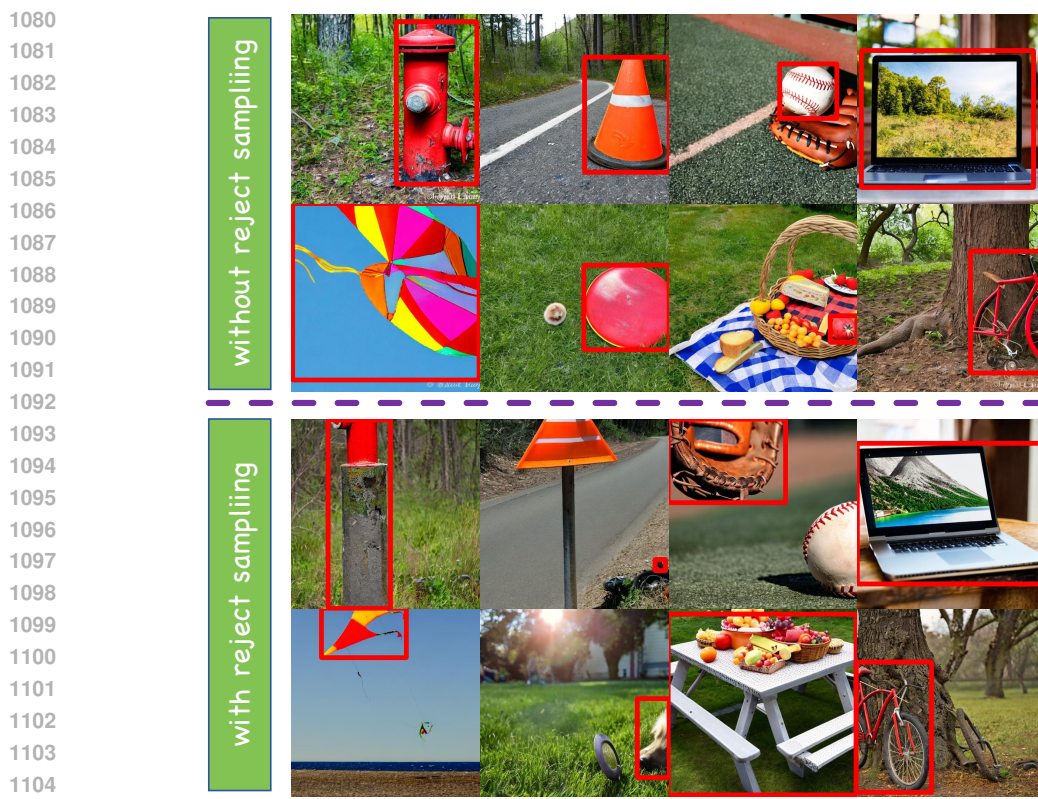


Figure 11: We visualize the generated images in the location diversity application in Sec 5.1. The upper part shows the results generated by one noise without rejection sampling, and the objects tend to cluster to the right edge of the picture. Then we generate a noise with no obvious trigger patch with the help of the detector obtained in Sec 3 and the reject sampling technique. The bottom part shows the results generated by that enhanced noise, which shows great diversity in object location.

**Visualized results** Please refer to the Fig 12 for visualized results.

## G MULTIPLE OBJECTS

We conducted additional experiments to assess our method’s ability to handle multiple objects. Following the protocol outlined in Attend-and-Excite Chefer et al. (2023), we used the same prompts provided in their GitHub repository and generated 64 images for each prompt. Below are some examples of the prompts used:

### Testing prompts

1. a lion and a yellow clock.
2. a bird and a black bowl.
3. a monkey and a red car.
4. a mouse with a bow.
5. a frog and a purple balloon.

For our method, we place two separate trigger patches on the left and right sides of the image. This allows us to prevent the two objects from fusing into each other. Specifically, the latent has a size of  $64 \times 64$ . We place the two trigger patches within the bounding boxes defined by the coordinates  $(0, 20, 24, 44)$  and  $(40, 64, 24, 44)$ , where the four coordinates represent the top-left and bottom-right corners of each bounding box in the format  $(x_1, x_2, y_1, y_2)$ . This ensures that the patches are placed in distinct regions of the image, preventing any overlap or fusion of the objects associated with these triggers.

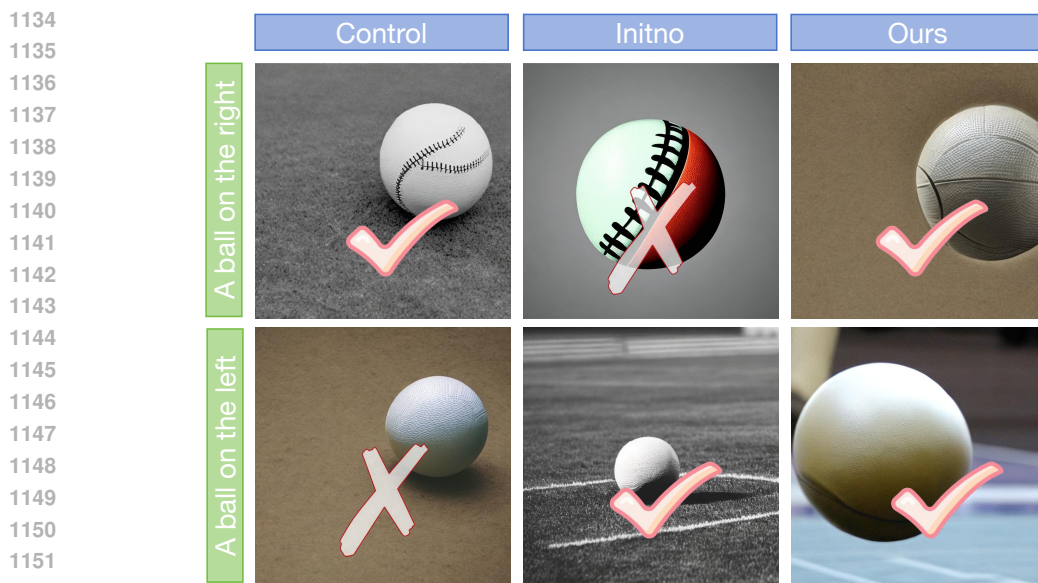


Figure 12: Visualization results of better prompt following application by injecting trigger patches in Sec 5.2. A check mark and a cross indicate whether the generated image is correct or not, respectively.

We adopt Composable Diffusion Liu et al. (2022b), Structure Diffusion Feng et al. (2022), Attend-and-Excite Chefer et al. (2023) and Divide-and-Bind Li et al. (2023) as our baselines. Please refer to Fig 13 for more visualized results.

We then evaluated the results using three metrics following the protocol in Attend-and-Excite Chefer et al. (2023): CLIP Full Image-Text Similarity (CLIP-Full), CLIP Minimum Image-Text Similarity (CLIP-Min), and BLIP-CLIP Text-Text Similarity (BLIP-Text), as proposed in the paper. We also utilize a human-preferred model, PickScore Kirstain et al. (2023) by comparing the results of these methods against the control baseline. The score reflects the model’s preference for the images generated by each method relative to the baseline. For all these metrics, **higher values indicate better performance**.

The results are as follows:

Table 12: Comparison of CLIP and BLIP-Text metrics for different methods.

Metrics	CLIP-Full	CLIP-Min	BLIP-Text	PickScore
Stable Diffusion	0.341	0.251	0.792	0.500
Composable Diffusion	0.348	0.252	0.768	0.514
Structure Diffusion	0.349	0.246	0.780	0.527
Attend-and-Excite	0.352	0.263	<b>0.830</b>	0.514
Divide-and-Bind	0.349	0.261	0.822	0.534
Ours	<b>0.360</b>	<b>0.264</b>	0.826	<b>0.557</b>

In the CLIP-Full, CLIP-Min and Pickscore metrics, our method achieved the best results, surpassing the strongest baselines designed for this task by 0.008 and 0.001, respectively. Additionally, our method does **not require any intervention in the attention maps** during the generation process, significantly reducing the computational resources needed and making it both model and prompt agnostic.

## H FAILED ANALYSIS FOR THE TRIGGER-PROMPT INTERACTION.

There are mainly three reasons for the failed cases of aligned experiments.

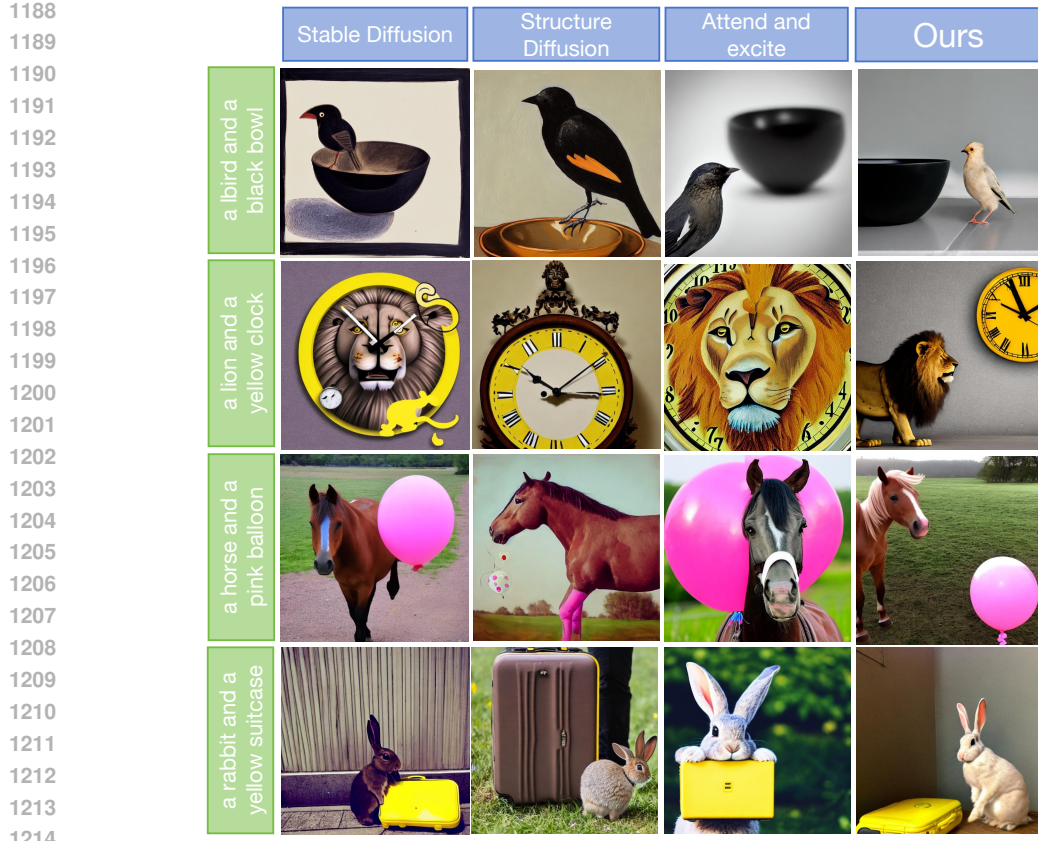


Figure 13: Visualized results of multiple objects generation.



Figure 14: Visualized results of the duplicate phenomenon.

Firstly, since our trigger patches are universal, any object can be generated at the designated position. Occasionally, irrelevant objects may occupy this position. For instance, given the prompt “a stop sign in the street” with the trigger patch located in the right corner, the position might instead be occupied by a tree. Please refer to Fig 16 for the visualized results.

Secondly, some classes we use have difficulty determining whether they are on the left or right. For example, for the class “fork,” the model often generates a long fork that stretches across the image horizontally.

Finally, in some cases, the objects are placed almost in the middle of the image and It is hard to judge if it is correct. These two cases will be categorized into “hard to judge”.

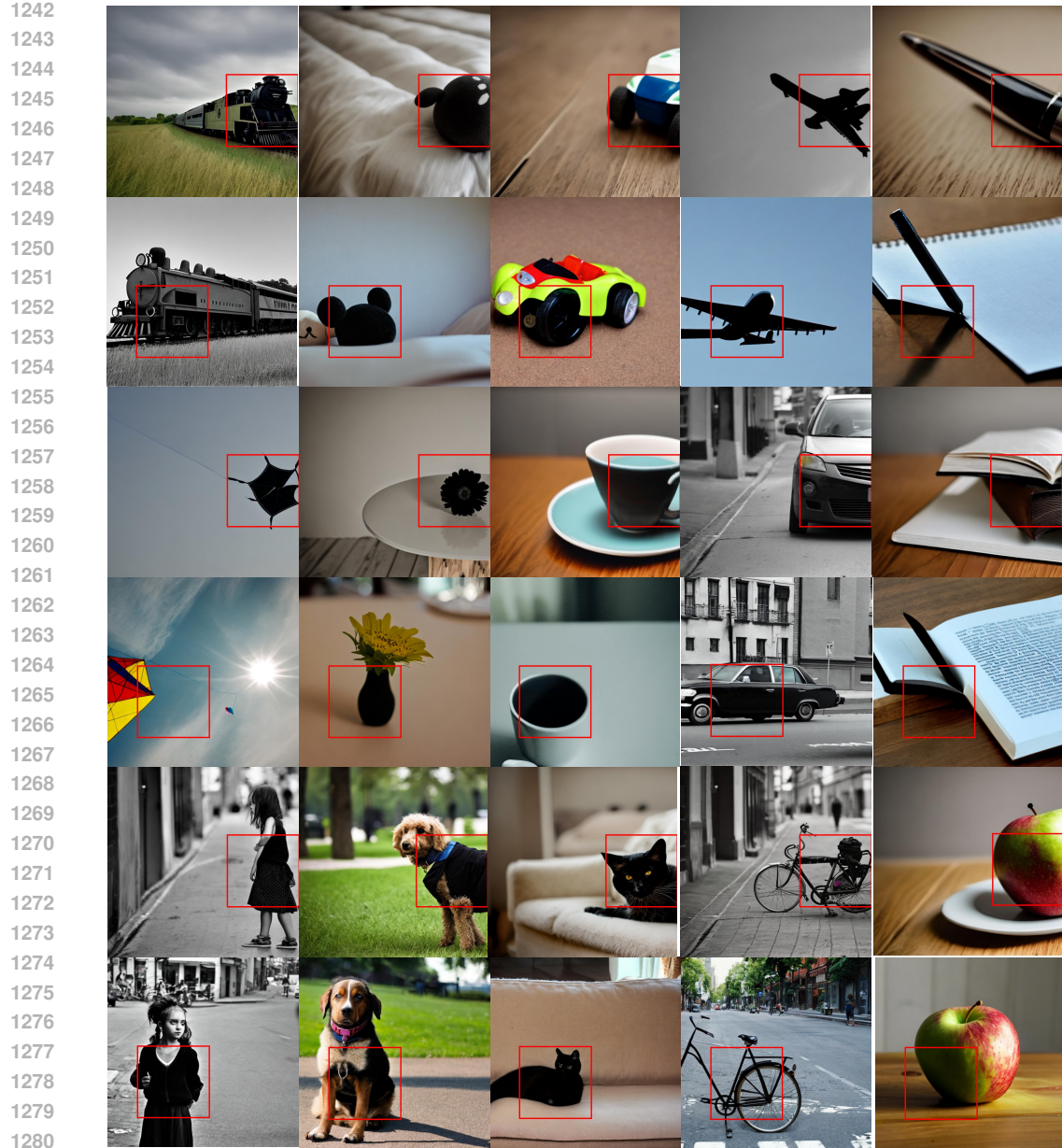


Figure 15: More examples to verify the generalization ability of the trigger patch for Fig 1. The first, third, and fifth rows display images generated from the same noise pattern, while the second, fourth, and sixth rows are derived from a blended noise pattern. Each pair of adjacent rows shares the same prompt. Within the red box, the "trigger patch" can be observed, showcasing its tendency to influence object generation. When this trigger patch is incorporated into the blended noise pattern, objects emerge in the corresponding positions in the images generated from the mixed noise.

We can observe that although “aligned” only has 63.5% , most of the rest samples belong to “hard to judge”, and there are very few samples belonging to “contradicted” and “duplicated”. In fact, if we ignore the hard-to-judge cases, there are 83.4% cases belonging to “aligned” while only 16.6% cases belong to “contradicted” and “duplicated”.

1296  
 1297  
 1298  
 1299  
 1300  
 1301  
 1302  
 1303  
 1304  
 1305  
 1306  
 1307  
 1308  
 1309  
 1310  
 1311  
 1312  
 1313  
 1314  
 1315  
 1316  
 1317  
 1318  
 1319  
 1320  
 1321  
 1322  
 1323  
 1324  
 1325  
 1326  
 1327  
 1328  
 1329  
 1330  
 1331  
 1332  
 1333  
 1334  
 1335  
 1336  
 1337  
 1338  
 1339  
 1340  
 1341  
 1342  
 1343  
 1344  
 1345  
 1346  
 1347  
 1348  
 1349

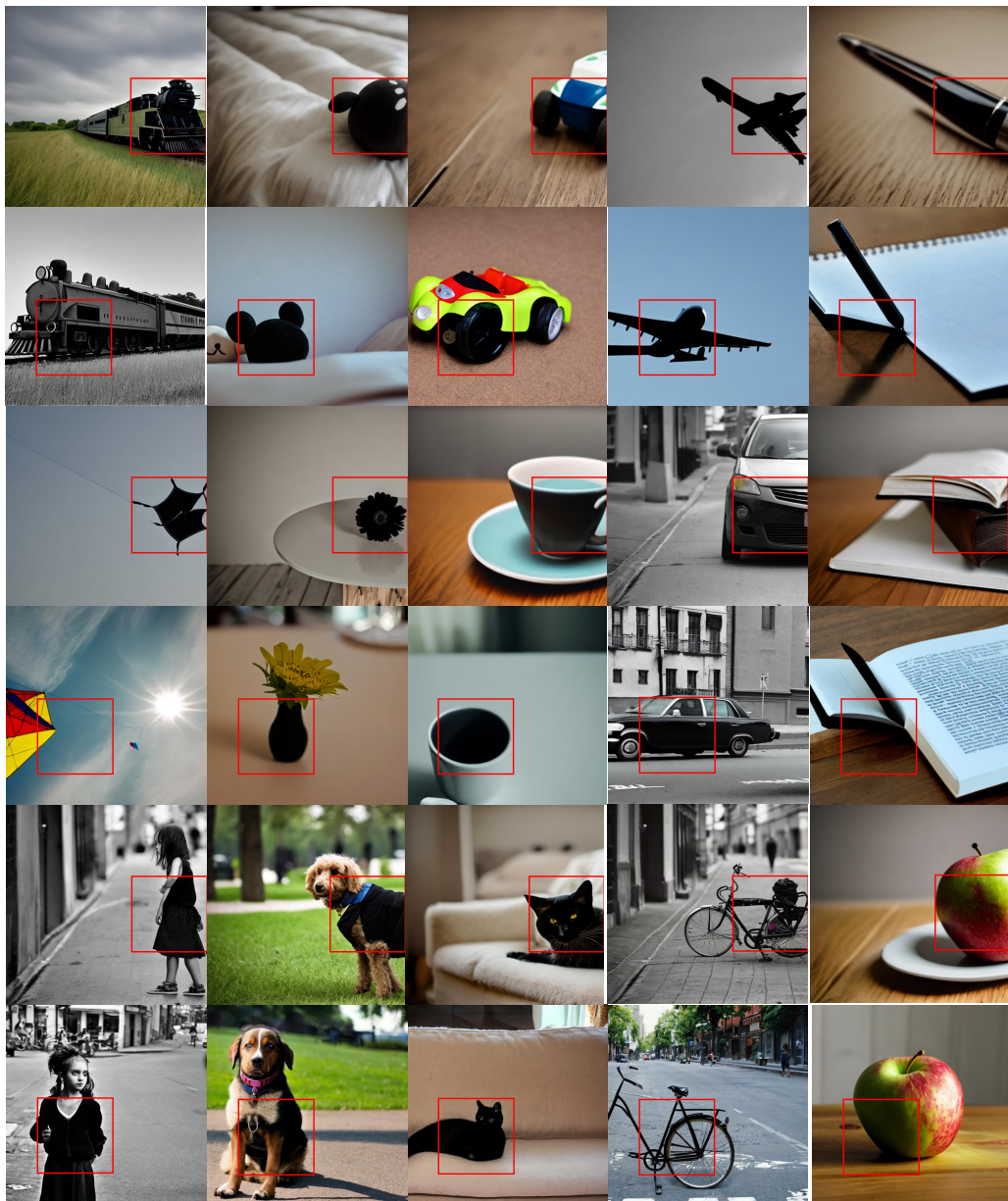


Figure 16: Failure analysis when the prompt aligns with the position of the trigger patch. In this case, there is a strong trigger patch located on the right edge of the image, while the prompt is “a stop sign on the right”. However, the tree and the stop sign often appear together., leading to occasional instances where the tree occupies the intended position of the stop sign.